


Multifunctional biocompatible films based on pectin-Ag nanocomposites and PVA: Design, characterization and antimicrobial potential

Aliaksandr Kraskouski¹  | Kseniya Hileuskaya¹ | Alena Ladutska² |
Volha Kabanava^{1,3} | Aliaksandr Liubimau⁴ | Galina Novik² |
Tran Thi Y. Nhi⁵ | Vladimir Agabekov¹

¹Department of Physicochemistry of Thin Film Materials, Institute of Chemistry of New Materials of NAS of Belarus, Minsk, Belarus

²Microbial Collection Laboratory, Institute of Microbiology of NAS of Belarus, Minsk, Belarus

³Department of Higher Mathematics and Mathematical Physics, Belarusian State University, Minsk, Belarus

⁴Department of Polymer Composite Materials, Belarusian State Technological University, Minsk, Belarus

⁵Laboratory of Natural Polymer, Institute of Chemistry of Vietnamese Academy of Science and Technology, Hanoi, Vietnam

Correspondence

Aliaksandr Kraskouski, Department of Physicochemistry of Thin Film Materials, Institute of Chemistry of New Materials of NAS of Belarus, 36 F. Skaryna Str., 220141 Minsk, Belarus.

Email: aleks.kraskovsky@gmail.com

Funding information

Vietnamese Academy of Science and Technology, Grant/Award Number: QTBY01.01/21-22; Belarusian Republican Foundation for Fundamental Research, Grant/Award Number: B21V-002/01

Abstract

Pectin-Ag nanocomposites with a core-shell structure are synthesized by the “green chemistry” method based on the reduction of silver nitrate with pectin (amidated, low-, or high methoxylated) in an alkaline medium at room temperature. TEM and DLS measurements show that the average size of the inorganic core (10–30 nm) and hydrodynamic diameter of the nanocomposite (284.8–649.2 nm) depend on the type of pectin. The films based on pectin-Ag nanocomposites and polyvinyl alcohol (PVA) with different molecular weight (30, 66, and 145 kDa) are obtained by casting evaporation technique. A comparative study of their mechanical, optical, degradation and antibacterial properties is carried out. The films with the smaller size of Ag nanocomposite exhibit higher antimicrobial activity against *Bacillus* strains. The pectin-Ag/PVA films are loaded with antibiotic kanamycin (KAN). Prolonged release of antibiotic and pronounced (up to full inhibition) antimicrobial effect of pectin-Ag/PVA/KAN films against *Escherichia coli*, *Pseudomonas aeruginosa*, *Bacillus pumilus*, and *Bacillus subtilis* is due to the formation of pectin-Ag/KAN complexes. Moreover, pectin-Ag/PVA/KAN films show high potency against resistant strains *Pseudomonas aeruginosa*. The obtained multifunctional films are expected to find promising applications in biomedical engineering and wound healing.

KEYWORDS

biomedical applications, films, kanamycin, pectin, silver nanoparticles

1 | INTRODUCTION

The worldwide escalation of bacterial multi-drug resistance (to conventional medical antibiotics) is a serious challenge to modern medicine and veterinary science. The spread of infections is a growing problem in most countries, aggravated by the development of microbial

resistance to antibiotics and disinfectants. Bacterial drug resistance causes dramatic problems in the prevention and treatment of infectious diseases.¹

One of the promising approaches to overcome bacterial resistance is the use of metallic nanoparticles,^{2–6} for example silver nanoparticles (AgNPs). Silver nanoparticles are effective antimicrobials⁷ and promising disinfectant.⁸ It

was found in comparative experiment that nanosilver is superior in antibacterial activity to other antimicrobial agents (titanium dioxide, polysilazane, zinc pyrithione etc.).⁹ Nowadays, different physical and chemical strategies and technologies for AgNPs synthesis have been described.^{10–14} Synthesis of AgNPs by physical methods (evaporation-condensation, laser ablation, electrical irradiation, gamma irradiation, and lithography) usually requires the extremely high temperature, vacuum conditions, and expensive equipment.^{15–17} Chemical methods, on the one side, are the most common methods because of their convenience (simple and mild conditions) and simple equipment, and on the other side, are usually need multiple steps and utilization of environmentally hazardous waste.” Green chemistry” methods are preferential to chemical and physical ones as more cost-effective and eco-friendly.^{18,19} Generally, in green synthesis metal ions form NPs that are stabilized using biological entities in aqueous solutions at ambient temperatures, neutral pH and eco-friendly conditions.^{18,19} Plant extracts as biological entities possess valuable properties (antihyperglycemic, antioxidant, antimutagenic, antifungal, anti-inflammatory, antiviral and antibacterial) which may be expressed in the biological activities of the final colloidal solution containing silver nanoparticles with potential medical applications²⁰ (e.g., in the wound healing as shown in²¹). However, multicomponent and variable composition of plant extracts does not enable to obtain nanoparticles with controlled properties (size, shape, and charge). The individual natural biopolymers such as polysaccharides allow to avoid these drawbacks. The multifunctional biopolymers can be considered as smart materials due to the presence of various functional groups (anionic and cationic, hydrophilic and hydrophobic) on the polymer skeleton, the activating key for which is external physicochemical stimuli (pH, temperature, ionic strength, etc.). Thus, the authors²² reported that lignin is intelligent nano-engineer (reducer and stabilizer) for synthesis of size and shape regulated silver, gold and palladium nanoparticles. In other work,²³ alkali-activated dextran was used as nanogenerator and protector for synthesis of metallic gold, silver and palladium nanoparticles. Moreover, bi- and multi-metal particles could also be obtained using polysaccharides. Ahmed et al.²⁴ proposed the energy saving method to fabricate 58.8 nm of Ag–Au–Pd catalytically active ternary core-shell nanostructures with promising applicability in water treatment using alginic acid as stabilizer. Emam et al.²⁵ applied arabic gum as bio-synthesizer of antibacterial Ag–Au nanocomposite by quite simple, energy saving and cost effective method. And hydroxyethyl cellulose was also used to synthesize monometallic and bimetallic antipathogenic Au–Au nanostructures.²⁶ In most cases, syntheses are thermally induced: the efficiency of silver ion reduction increases with increasing temperature. Moreover, the thermo chemical reduction of silver is possible not only

in solutions of polysaccharides, but also in films of polyelectrolyte complexes based on biopolymers.²⁷ The authors proved the mechanism of thermally induced reduction of silver by polyelectrolyte complexes consists in the formation of an Ag^+ bond with the carboxyl groups of the polyanionic component of the film and their subsequent reduction due to the oxidation of the hydroxyl groups in the glucopyranose units of the polycationic components (chitosan, functionalized cyclodextrin, and starch). The synthesized monometallic and multimetallic bionanocomposites exhibit antibacterial and antifungal activity,^{26,27} and also have the potential to be used in the remediation of pesticides and as an effective recyclable catalyst.²⁸

Pectin is a polyanionic biodegradable and biocompatible natural polysaccharide formed from residues of D-galacturonic acid in the pyranose form linked by α -1,4-glycosidic bonds. Pectin exhibits anti-inflammatory,²⁹ mucoadhesive,³⁰ antitumor,^{31,32} antimicrobial³³ properties and widely used in biomedical applications.³⁴ The presence of functional (carboxyl and hydroxyl) groups allows simultaneously to use of pectins as a reducing agent and stabilizer of gold³⁵ and silver nanoparticles.³⁶ At our previous study,³⁷ we have presented environmentally friendly technique to obtain aggregately stable negatively charged core-shell structured pectin-Ag nanocomposites by alkali-activated polymer as reducer and stabilizer at room temperature. Although the preparation of pectin-silver nanocomposites in an alkaline medium has been described in several works,^{35,38,39} the main advantage of our proposed technique is the synthesis of size-controlled nanoparticles due to the complete chemical reduction of silver ions by pectin without heating. The obtained pectin-silver nanocomposites are promising antibacterial materials for biomedical applications. Thus, Hussain et al. reported that functionalization of AgNPs with biopolymers showed promising improvement of their various biomedical properties such as wound healing, tissue regeneration, antibacterial, anti-inflammatory, and so forth.⁴⁰

Another effective way to overcome bacterial resistance is combining silver nanoparticles with antibiotics. These combinations are able to synergistically inhibit bacterial growth.^{41–45} Thus, Deng et al.⁴¹ found that enoxacin, kanamycin, neomycin, and tetracycline show synergistic growth inhibition against the multidrug resistant bacterium *Salmonella typhimurium* when combined with AgNP. According to Patra et al.⁴³ the AgNPs displayed positive antibacterial activity against different foodborne pathogenic bacteria, as well as strong synergistic antibacterial activity with low concentrations of kanamycin or rifampicin. In study,⁴⁴ authors demonstrated that a combination of AgNPs with either gentamicin or neomycin showed synergistic antibacterial properties in *Staphylococcus aureus* isolates from mastitis.

Thin-film materials are frequently used in clinical therapy of wounds and skin lesions.^{46,47} Antimicrobial

TABLE 1 SPR maxima of the pectin-Ag nanocomposites, pectin-Ag/PVA and pectin-Ag/PVA/KAN films

Molecular weight of PVA	SPR maxima (nm)		
	Type of nanocomposite		
	Citrus-Ag	Classic-Ag	Amid-Ag
Nanocomposite			
—	412	410	415
Film			
30,000	429	445	435
66,000	426	441	443
145,000	424	442	441
Kanamycin-containing film			
30,000	413	425	421
66,000	413	420	422
145,000	415	422	420

Abbreviation: PVA, polyvinyl alcohol.

coatings and films with active ingredients could be reliable tools for active killing of microorganisms.⁴⁸ Metal nanoparticles as mentioned above (Ag,⁴⁹ Au,⁵⁰ Cu,⁵¹ ZnO,⁵² TiO₂,^{51,53} etc.) as well as common antiseptics^{54,55} and antibiotics,^{56,57} natural biological active substances^{58–60} are widely applied as effective antimicrobial components of such films. Polyvinyl alcohol (PVA) is one of the synthetic, water-soluble, biodegradable, biocompatible, film forming material^{61–64} often engaged as a basis of wound dressings, artificial skin and transdermal patches.^{46,65} Moreover, it shows excellent mechanical properties.⁶⁶ Nevertheless, the aspects of preserving antibacterial potential of silver nanoparticles in thin PVA films remains the subject of additional studies. Furthermore, there are few and fragmentary literature data on the properties of PVA-nanobiocomposite-antibiotic multicomponent films, the features of the interaction of the components and the relationship between the composition of the films and their biological properties.

In this paper, we describe preparation and properties of polymer films, including kanamycin-loaded ones, based on pectin-Ag nanocomposites. We carried out a comparative analysis of the physicochemical characteristics and antibacterial properties (including against antibiotic-resistant strains) of the obtained films.

2 | RESULTS AND DISCUSSION

2.1 | Characterization of pectin-Ag nanocomposites

At previous study,³⁷ we reported that synthesized pectin-Ag nanocomposites are hydrosols of AgNPs stabilized by a shell of pectin. The presence of surface plasmon resonance

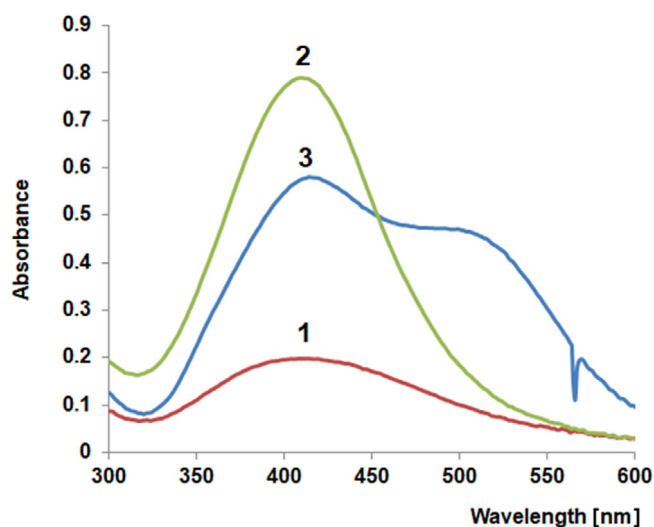


FIGURE 1 Ultra violet (UV)-visible absorption spectra of Citrus-Ag (1), Classic-Ag (2) and Amid-Ag (3) nanocomposites [Color figure can be viewed at wileyonlinelibrary.com]

band in the region of 410–415 nm in the absorption spectra of synthesized pectin-Ag nanocomposites indicates the presence of Ag⁰ nanoparticles (Table 1, Figure 1).

The pectin-Ag nanocomposites had a spherical shape with the average diameter of nanoparticles <50 nm (Figure 2) and negative ζ -potential values (40 ÷ 50 mV). The size of AgNPs decreases in Amid-Ag–Citrus-Ag–Classic-Ag series (Figure 2). It is known³⁶ that the size and structure of pectin-Ag nanoparticles depend on the type and number of functional groups (OH, COOH, and NH₂) of the polymer, which in turn predetermine the reducing and stabilizing potential of the polysaccharide. Thus, non-amidated pectins are characterized by the fastest reduction rate of silver ions, which promotes the yield

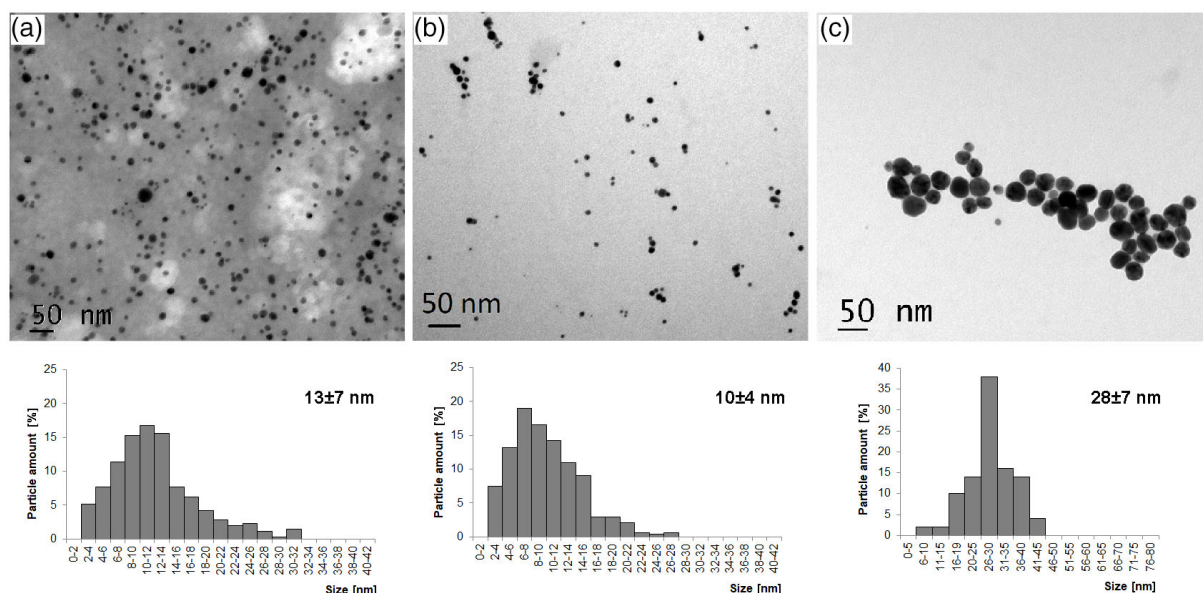


FIGURE 2 Transmission electron microscopy (TEM)-images and size distribution of Citrus-Ag (a), Classic-Ag (b) and Amid-Ag (c) nanocomposites³⁷

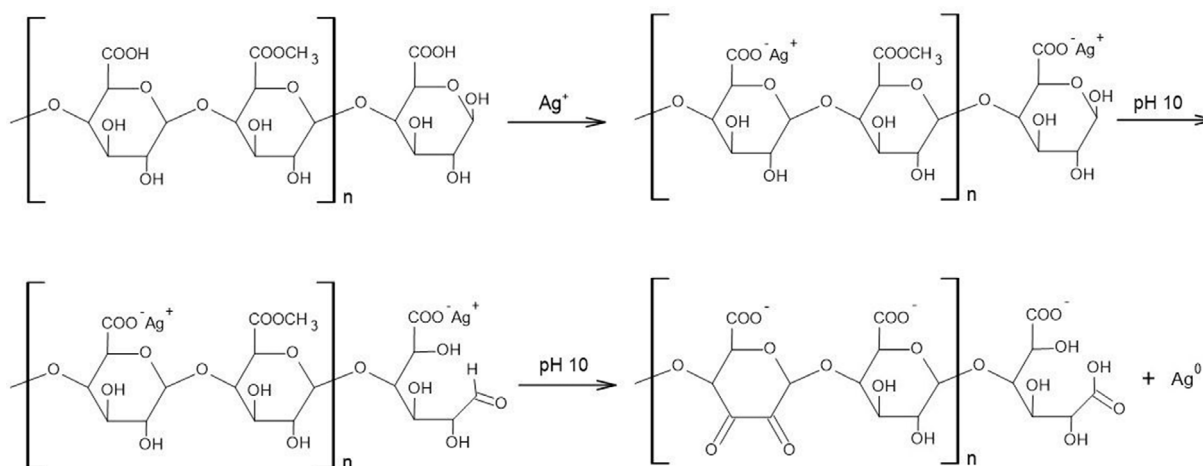


FIGURE 3 Scheme of reduction of silver ions with pectin

of a large number of crystal nuclei, resulting in the formation of single small-sized nanoparticles.^{36,37}

2.2 | Mechanism of reduction of silver ions

In this study, pectins with different degrees of esterification and amidation were used to reduce silver ions. As we showed earlier^{36,37} the mechanism of reduction of silver cations by pectin consists of two stages (Figure 3).

At the first stage, silver ions react with the carboxyl groups of the polysaccharide to form a salt (silver pectinate). Moreover, additional hydrogen bonds are formed

due to the participation of the hydroxyl groups of the glucopyranose ring and amide groups (in the case of amidated pectin), fixing Ag^+ on the polymer chains. At the second stage, the chemical reduction of silver ions by the functional groups of pectin occurs. It should be noted that in an alkaline medium the reducing hemiacetal hydroxyl groups of pectin are activated, which, along with the secondary hydroxyl groups of arabinan, galactan, and D-galacturonic acid fragments of pectin, participate in the reduction reaction, being oxidized to ketones. Simultaneously, the base-catalyzed hydrolysis (saponification) of ester groups of the methoxylated pectin molecule occurs, and free carboxyl groups formed, along with the free hydroxyl groups of the ring, participate in the

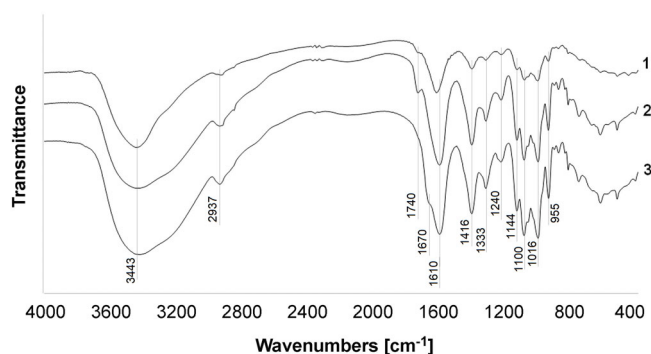


FIGURE 4 Fourier transform infrared (FTIR) spectra of pectin-Ag nanocomposites (1–Citrus-Ag, 2–Classic-Ag, 3–Amid-Ag)

stabilization of the synthesized metal nanoparticles. A similar mechanism of participation of hydroxyl groups of glucopyranose rings of polysaccharides in the reduction of silver ions was also described by the authors⁶⁷ in the synthesis of pectin-silver hydrosols and the thermochemical synthesis of silver nanoparticles in interpolyelectrolyte complexes.^{27,68} At the same time, the authors proved that the high temperatures lead to a deeper oxidation reaction of the secondary hydroxyl groups of the ring to aldehyde and carboxyl groups, which causes structural degradation of the polysaccharide.

2.3 | FTIR spectroscopy of pectin-Ag nanocomposites

Fourier transform infrared (FTIR) spectra of pectin-Ag nanocomposites in 4000–400 cm^{-1} range are shown in Figure 4. The broad band at 3443–3423 cm^{-1} and weak band at 2937–2926 cm^{-1} are assigned to the vibration of $-\text{OH}$ groups and $\nu(\text{C}-\text{H})$, respectively.^{69,70} The intense bands at 1630–1610 and 1416 cm^{-1} are related to $\nu_{\text{as}}(\text{COO}^-)$ and $\nu_{\text{s}}(\text{COO}^-)$. The deformation vibrations $\text{C}-\text{H}$ and $\text{O}-\text{H}$ group in the pyranose rings of the pectin chain appear at 1333–1331 and 1240–1238 cm^{-1} .^{37,69,71} Few peaks at 1200–1000 cm^{-1} (main maxima: 1144, 1100, and 1016 cm^{-1}) correspond to $\nu(\text{C}-\text{O}-\text{C})$ glycosidic bonds and $\nu(\text{C}-\text{C})(\text{C}-\text{O})$ of the ring. The bands at 955–953 cm^{-1} are attributed to $\delta(\text{COH})$ vibrations.⁷¹

In addition, FTIR spectra of pectin-Ag nanocomposites showed presence of the band at 1740 cm^{-1} corresponding to the stretching vibrations of the carbonyl group $\nu(\text{C}=\text{O})$ of the methyl ester (COOCH_3) or to the undissociated carboxyl group^{69,70,72} for Classic-Ag and Citrus-Ag and its absence for Amid-Ag. At the same time in FTIR spectra of Amid-Ag the weak band at 1670 cm^{-1} which is attributed to stretching vibrations of the $\nu(\text{C}=\text{O})$ of the amid group was observed.

2.4 | Characterization of pectin-Ag/PVA films

The resulting pectin-Ag/PVA films are transparent (Table 2), have a smooth uniform morphology and a color from orange-yellow to brown-red (Figure 5). The Classic-Ag/PVA and Citrus-Ag/PVA films have a high transparency ($\geq 84\%$) except for Citrus-Ag/PVA 30000 film, which has a lowest transparency (31%). This effect can be explained by sweating-out of plasticizer during storage due to weaker hydrogen bonding between Citrus-Ag and PVA 30000, which is consistent with the spectroscopic data for Citrus-Ag/PVA 30000 films: the SPR maximum shift ($\Delta 17$ nm) was the smallest (Table 1). Moreover, glycerin diffuses more easily to the surface of film based on low molecular weight PVA compared to high molecular weight polymer due to less steric hindrance. The decrease in transparency of the film by sweating-out of glycerol was also observed for mung bean starch/guar gum,⁷³ poly(lactide)/whey protein,⁷⁴ and alginate⁷⁵ films. The obtained data indicate good compatibility between PVA and pectin-Ag nanocomposites, which might result from their strong hydrogen-bond interaction. The Amid-Ag/PVA films are less transparent in comparison with Classic-Ag/PVA and Citrus-Ag/PVA films (Table 2). This difference can be explained by higher light scattering due to the larger size of the Amid-Ag nanoparticles.

The weight of obtained films was 0.50 ± 0.02 g and the thickness < 50 μm (Table 3). The position and maximum of SPR band in the 424–445 nm region in the absorption spectra of the films (Figure 6) indicates preservation of the shape and size of Ag^0 nanoparticles (Table 1). In comparison with the initial hydrosols ($\lambda_{\text{max}} = 410$ –415 nm), a bathochromic shift of the SPR maximum of the films was observed (Figure 6). Probably, this shift was caused by the interaction of carboxyl groups of pectin macromolecules and hydroxyl groups of PVA and changes in the AgNPs environment.⁶⁹

2.5 | FTIR spectroscopy of PVA and pectin-Ag/PVA films

The neat PVA films showed (Figure 7) main bands at 3281, 2937–2910, 1711, 1657, 1418, and 1327 cm^{-1} which are attributed to the $\nu(\text{OH})$, $\nu(\text{CH}_2)$, $\nu(\text{C}=\text{O})$, $\delta(\text{OH})$, $\delta(\text{CH}-\text{OH})$, $\delta(\text{CH} + \text{OH})$, respectively. The other characteristic bands at 1142, 1094, and 1036 cm^{-1} are related to $\nu(\text{C}-\text{O})$.⁷⁶

In FTIR, spectra of pectin-Ag/PVA films all characteristic peaks of PVA were preserved (Figure 7). New intense bands appear at 1650–1600 cm^{-1} and correspond to vibrations of carbonyl groups $\nu(\text{COO}^-)$ of pectin macromolecules in pectin-Ag nanocomposite. Also, in comparison with initial components (PVA and nanocomposites) the band

Molecular weight of PVA	Transmittance (%)		
	Type of nanocomposite		
	Citrus-Ag	Classic-Ag	Amid-Ag
30,000	31 ± 4	86 ± 5	54 ± 5
66,000	93 ± 4	84 ± 3	74 ± 2
145,000	91 ± 3	95 ± 5	72 ± 4

TABLE 2 Transparency of the pectin-Ag/PVA films

Abbreviation: PVA, polyvinyl alcohol.

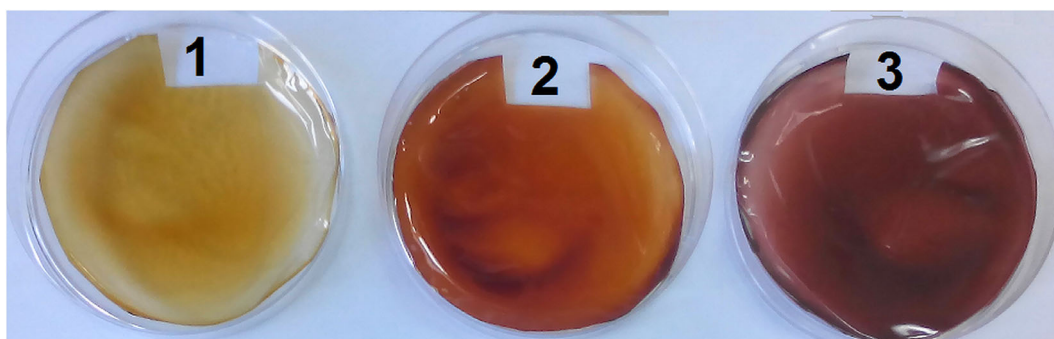


FIGURE 5 The image of the films based on pectin-Ag nanocomposites (1–Citrus-Ag, 2–Classic-Ag, and 3–Amid-Ag) and PVA 30,000 [Color figure can be viewed at wileyonlinelibrary.com]

TABLE 3 Mechanical properties of pectin-Ag/PVA films

Pectin-Ag nanocomposite	Tensile strength (MPa)	Percent elongation (%)	Young's modulus (MPa)	Thickness (μm)
PVA 30000				
Citrus-Ag	7.4 ± 1.0	27 ± 7	128.0 ± 45.9	46.0 ± 4.7
Classic-Ag	11.2 ± 1.7	43 ± 6	121.5 ± 20.3	45.0 ± 3.0
Amid-Ag	9.2 ± 1.7	25 ± 6	244.5 ± 55.0	32.7 ± 2.3
PVA 145000				
Citrus-Ag	14.0 ± 4.0	120 ± 22	93.5 ± 30.5	43.5 ± 3.8
Classic-Ag	18.2 ± 4.7	222 ± 19	72.1 ± 13.9	44.2 ± 4.3
Amid-Ag	14.5 ± 4.4	146 ± 36	70.0 ± 9.4	37.2 ± 3.2

Abbreviation: PVA, polyvinyl alcohol.

shifting (from 3281 cm⁻¹ in PVA and 3443–3423 cm⁻¹ in nanocomposites to 3265–3263 cm⁻¹ in pectin-Ag/PVA films) was detected (Figures 4 and 7). The bands at 3600–3200 cm⁻¹ are linked to the —OH groups involved in intra-molecular and intermolecular H— bonds. Therefore, FTIR peak shifting towards a lower wavenumber side indicates the strong H— bond interaction between PVA and pectin-Ag nanocomposite.⁶⁹

2.6 | Degradation of pectin-Ag/PVA films in PBS

The degradation of the films was studied in vitro in PBS (Figure 8). PBS was used as a system simulating

internal environment of the organism. The weight of the samples decreased by 30%–45% after 28 days of aging. During the first day of aging the maximum weight loss of the films was observed and it underwent no further changes with time. The degradation of the films did not depend on the type of nanocomposite, it was determined mainly by the molecular weight of PVA. Thus, weight loss decreased in the following series: pectin-Ag/PVA 30000–pectin-Ag/PVA 66000–pectin-Ag/PVA 145000. This might be due to a decrease in the solubility of PVA with an increase in its molecular weight.⁷⁷ Moreover, the main contribution to weight loss could be made by release of the glycerol containing in the film. The strong affinity of glycerol to water (due to the hydrophilic nature of

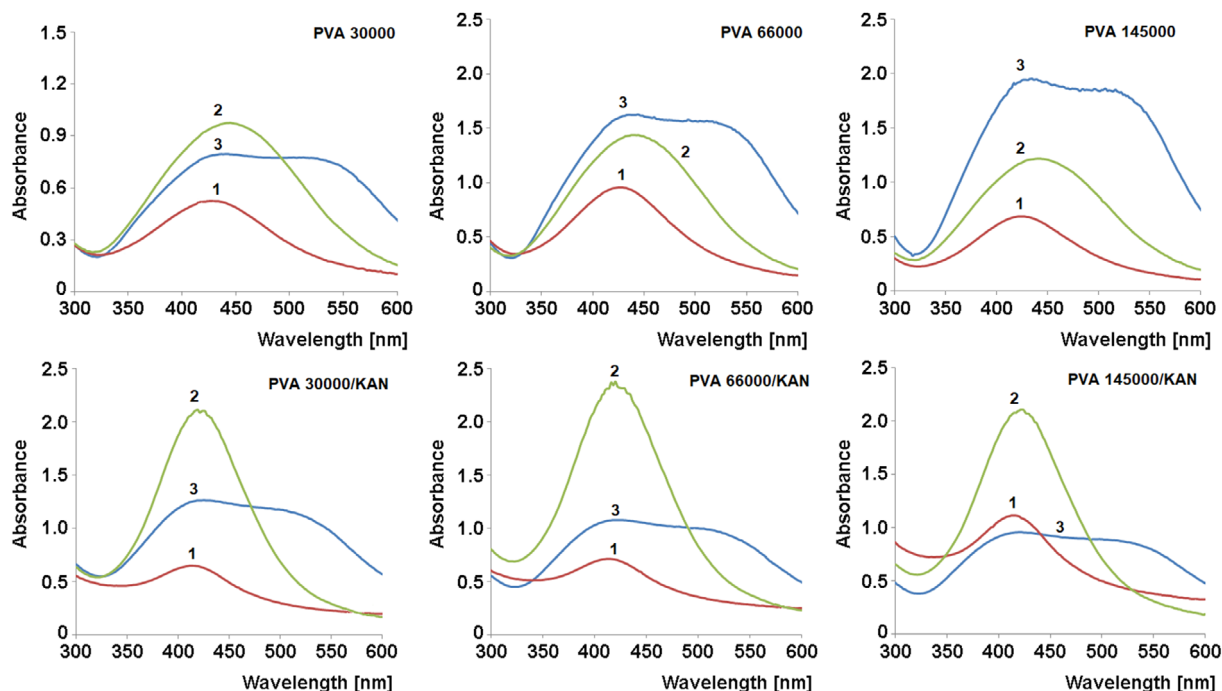


FIGURE 6 Ultra violet (UV)–visible absorption spectra of pectin-Ag/PVA and pectin-Ag/PVA/KAN films: 1–Citrus-Ag, 2–Classic-Ag, 3–Amid-Ag [Color figure can be viewed at wileyonlinelibrary.com]

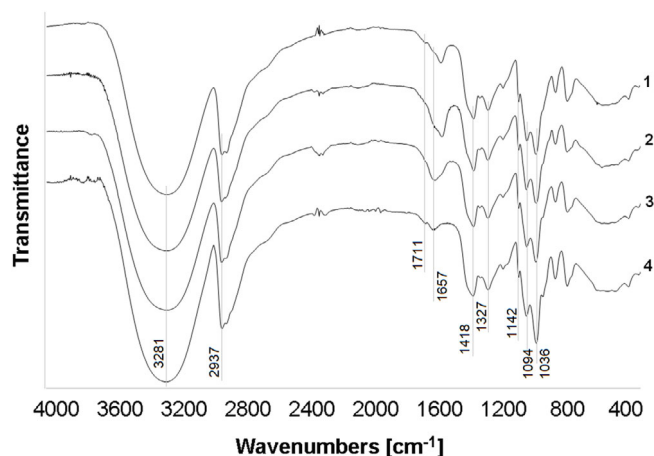


FIGURE 7 Fourier transform infrared (FTIR) spectra of polyvinyl alcohol (PVA) 145,000 film (4) and pectin-Ag/PVA films based on: 1–Citrus-Ag, 2–Classic-Ag, 3–Amid-Ag

plasticizer) acts as a strong driving force for leaching of glycerol from pectin-Ag/PVA film immersed in PBS. The similar effect was also observed for glycerol-containing films based on starch,⁷⁸ starch and chitosan,⁷⁹ starch and montmorillonite.⁸⁰ It should be noted that the final content of glycerol in the pectin-Ag/PVA film was 32.75 wt%, which corresponds with the minimum weight loss (~ 30 wt%) typical for films based on poorly soluble PVA 145000.

2.7 | Mechanical properties of pectin-Ag/PVA films

Mechanical properties of polymeric films are very important parameters for their medical and food applications. It was established that the mechanical properties of the pectin-Ag/PVA films were affected both by molecular weight of PVA and the type of nanocomposite (Table 3). Thus, the increase in the molecular weight of PVA led to the increase in the tensile strength by ~ 1.5 –2 times and the percent elongation by ~ 5 fold as well as the decrease in Young's modulus by ~ 1.5 –3 times. The high molecular weight PVA compared to low molecular weight has a larger number of hydroxyl groups capable to form of intra- and intermolecular hydrogen bonds, which cause the increase in tensile strength and the percent elongation of the films. The authors⁸¹ also reported that PVA with higher molecular weight improves tensile strength and elongation at break of fish myofibrillar protein/PVA blend films. It was found that the films based on PVA 145000 were more elastic.

The films based on Classic-Ag nanocomposite compared with other films had the highest values of tensile strength and elongation at break. It may be explained by stronger H— bond networks between functional groups (carboxyl and hydroxyl) of Classic-Ag and PVA. In fact, the analysis of FTIR spectra showed that Classic-Ag/PVA

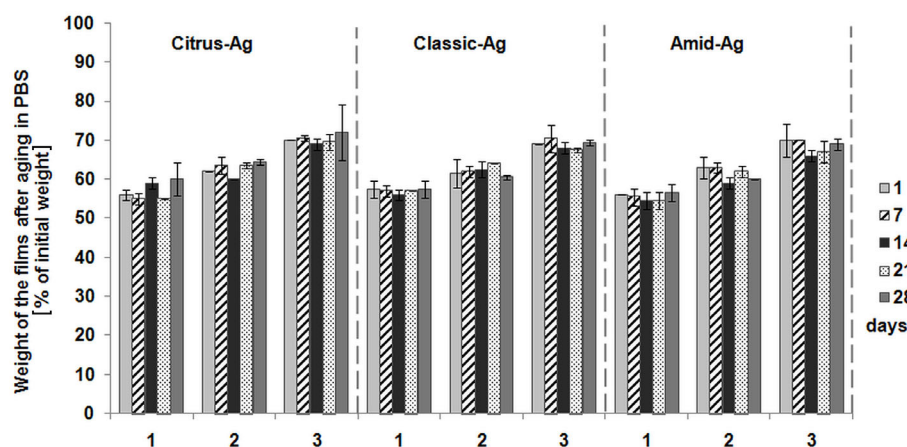


FIGURE 8 Degradation of pectin-Ag/PVA films in PBS: 1–PVA 30000; 2–PVA 66000; 3–PVA 145000

TABLE 4 Characteristics of pectin-Ag nanocomposites and pectin-Ag/KAN complexes

	Citrus-Ag	Classic-Ag	Amid-Ag	Citrus-Ag/KAN	Classic-Ag/KAN	Amid-Ag/KAN
ζ -potential (mV)	-42.5 ± 1.0	-41.5 ± 1.2	-47.1 ± 0.6	-25.5 ± 2.7	-23.7 ± 0.5	-21.7 ± 2.6
d_H (nm)	356.8 ± 8.1	649.2 ± 58.5	284.8 ± 45.8	466.5 ± 29.1	773.8 ± 44.3	384.2 ± 35.1

film had the most intense band of carbonyl vibrations at 1608 cm^{-1} (Figure 7), indicating that Classic-Ag nanocomposite possessed more number of carboxyl groups capable to form hydrogen bonds with PVA macromolecules. These data corresponds with the results of SPR analysis: the most significant bathochromic shift ($\Delta 31\text{--}35\text{ nm}$) was observed in films based on Classic-Ag. Therefore, on the one hand, the formation of crosslinking network via H— bonds of Classic-Ag and PVA increased the tensile strength of these films and, on the other hand, improved their flexibility.

2.8 | Interaction between pectin-Ag nanocomposites and kanamycin

The absolute value of ζ -potential of AgNPs decreases in 1.7–2.2 times (Table 4) upon addition of kanamycin to pectin-Ag hydrosols due to electrostatic interaction of negatively charged carboxyl groups of pectin and positively charged amino groups of antibiotic. Furthermore, the increase of hydrodynamic diameter of AgNPs compared with initial one in 1.2–1.4 times was observed, which also confirms the interaction of pectin-Ag with the antibiotic. The change of d_H was apparently caused by the loosening of the polymer shell of the nanocomposite by entrapment of kanamycin. It should be noted that the hydrodynamic diameter of nanocomposites changes in the series $\text{Amid-Ag} < \text{Citrus-Ag} < \text{Classic-Ag}$ and this phenomenon was also observed for pectin-Ag/KAN (Table 4).

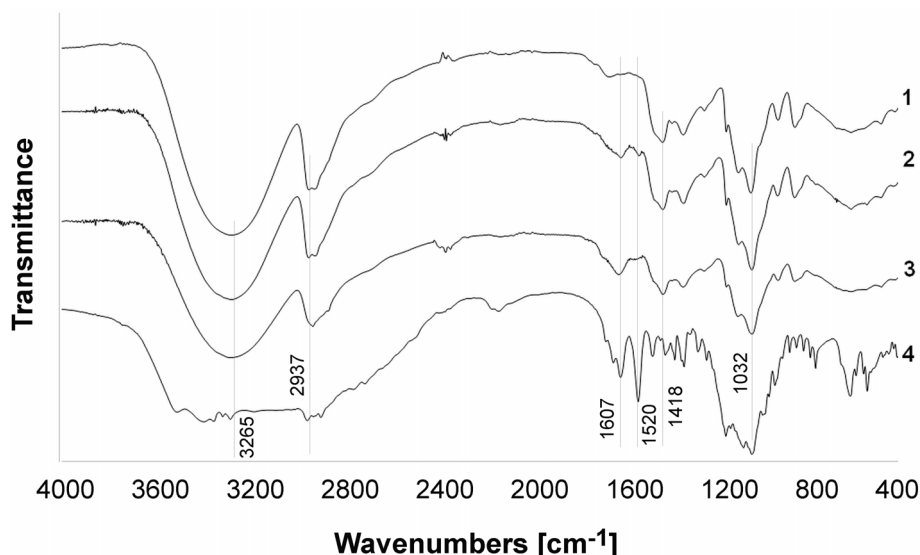
2.9 | FTIR spectroscopy of pectin-Ag/KAN complexes

Fourier transform infrared (FTIR) spectra of pectin-Ag/KAN samples in $2000\text{--}1000\text{ cm}^{-1}$ range are shown in Supplementary Information (SI). It should be noted that in contrast to FTIR spectra of pectin-Ag nanocomposites, a new band of vibrations appeared at $1535\text{--}1529\text{ cm}^{-1}$ (SI). This band attributes to deformation vibrations of NH_3^+ group of kanamycin. The shift of peak position from 1520 cm^{-1} (pure kanamycin) was detected. Also the peak position of COO^- groups at $1630\text{--}1610$ was shifted (SI). These changes in FTIR spectra is caused by intermolecular interaction of amino groups of KAN and carboxyl groups of pectin-Ag nanocomposite.⁷² Thus, obtained DLS and FTIR results indicate that pectin-Ag nanocomposite forms a complex with kanamycin.

2.10 | Characterization of kanamycin-containing pectin-Ag/PVA films

The thickness of pectin-Ag/PVA films containing kanamycin was $67.3 \pm 7.5\text{ }\mu\text{m}$. The content of antibiotic in the film was $\sim 15\text{ wt\%}$. The obtained films were transparent, without pores or cracks and were colored from lemon yellow to brown-red depending on the type of pectin-Ag nanocomposite. When kanamycin was added a hypsochromic shift of the SPR maximum in the ultra violet (UV)–Vis spectra of the films was observed (Table 1). It may be attributed to the interaction of the carboxyl

FIGURE 9 Fourier transform infrared (FTIR) spectra of KAN (4) and pectin-Ag/PVA 145000/KAN films based on: 1–Citrus-Ag, 2–Classic-Ag, 3–Amid-Ag



groups of pectin and the amino groups of kanamycin, that is, formation of the pectin-Ag/kanamycin complex due to electrostatic interaction, as evidenced by altered intensity of vibrations in the $1700\text{--}1600\text{ cm}^{-1}$ region in the FTIR spectra of the films (Figures 7 and 9). It should be also noted that in contrast to FTIR spectra of pectin-Ag/PVA films, a new weak band of vibrations appeared at $1544\text{--}1518\text{ cm}^{-1}$ in the FTIR spectra of pectin-Ag/PVA/KAN films (Figure 9), which may be correlated with the deformation vibrations of NH_3^+ group of kanamycin.⁸²

2.11 | KAN release from pectin-Ag/PVA films

The bioavailability of kanamycin entrapped into the pectin-Ag/PVA films did not decrease. The full release of the included KAN in 0.9% NaCl solution occurred during the first 180 min (Figure 10). The rate of KAN release from the films did not significantly depend on molecular weight of PVA and the type of nanocomposite.

2.12 | Antibacterial activity of pectin-Ag/PVA films against gram-positive bacteria strains

It was previously shown that pectin-Ag nanocomposites³⁷ and hydrogels⁴² based on them exhibited antimicrobial activity against gram-negative and gram-positive bacteria.

It was found that the obtained pectin-Ag/PVA films exhibited antibacterial activity against selected spore-forming bacteria of the genus *Bacillus*: strains *B. subtilis* BIM B-210, *B. pumilus* BIM B-211, *B. pumilus* BIM B-373 (Table 5). Bioactivity of the films was comparable or even

higher than kanamycin action (disk $30\text{ }\mu\text{g}$). The sole exception was bacterial strain *B. subtilis* BIM B-25 which was not sensitive to both pectin-Ag/PVA films and KAN.

It was shown that the control PVA films did not exhibit antibacterial activity. Therefore, the antimicrobial properties of pectin-Ag/PVA films against gram-positive bacteria were due precisely to the presence of pectin-Ag nanocomposite. In general, the highest growth-inhibiting effect was registered for films with Citrus-Ag nanocomposite. These results correspond with the previous data on nanocomposites alone: antimicrobial activity against gram-positive bacteria increased in Amid-Ag–Classic-Ag–Citrus-Ag series.⁴² Thus, the incorporation of the pectin-Ag nanocomposite in the polymer matrix of PVA with various molecular weights did not change its antibacterial activity.

The obtained results are well correlated with the literature data. Antibacterial activity increases with decrease in size of nanocomposite, and this effect was observed both for colloid silver hydrosols⁸³ and nanobiocomposites immobilized into films.^{68,84} The authors⁸⁴ also showed the enhanced activity of nanobiocomposites, immobilized on cellulose sheets, against gram-positive bacteria. The pectin-Ag/PVA films have demonstrated the efficiency of growth inhibition of gram-positive bacteria (Table 5) comparable or higher to PVA films incorporated with pre-synthesized by green method and using standard reducing agents (NaBH_4 /citrate) silver nanoparticles (the size of inhibition zone was $9\text{--}10$ and 7 mm for *S. aureus*, respectively)⁸⁵ and exceeded the activity of PVA films containing silver nanoparticles synthesized in situ⁸⁶ although the amount of silver in the prepared pectin-Ag/PVA films was less ($0.6\text{ wt}\%$).

It is known that the mechanism of the antibacterial action of silver nanoparticles is due to both the released

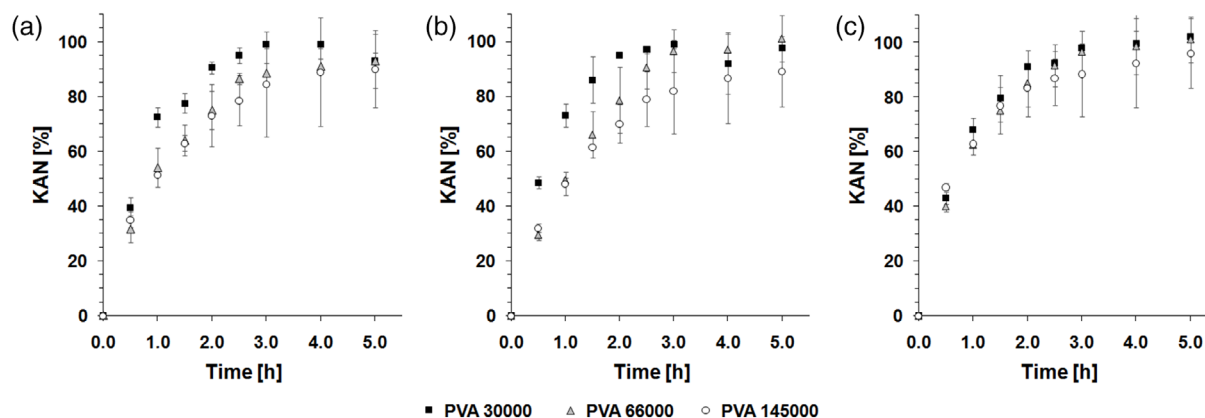


FIGURE 10 Kanamycin release in 0.9% NaCl solution from (a) Citrus-Ag/PVA, (b) Classic-Ag/PVA, and (c) Amid-Ag/PVA films

TABLE 5 Antibacterial activity of the pectin-Ag/PVA films

Film composition		Inhibition zone (mm)					
Pectin-Ag	Mw PVA	<i>B. subtilis</i> B-25	<i>B. subtilis</i> B-210	<i>B. pumilus</i> B-211	<i>B. pumilus</i> B-373	<i>P. aeruginosa</i> B-153	<i>E. coli</i> B-378
Citrus-Ag	30,000	2–3	12	12	12	N/A	N/A
	66,000	1–2	15	12	11	N/A	N/A
	145,000	2	12	12	12	N/A	N/A
Classic-Ag	30,000	N/A	9	12	16	N/A	N/A
	66,000	N/A	11	13	10	N/A	N/A
	145,000	N/A	13	12	13	N/A	N/A
Amid-Ag	30,000	N/A	11	10	12	N/A	N/A
	66,000	N/A	11	11	12	N/A	N/A
	145,000	N/A	14	11	15	N/A	N/A
Kanamycin (disk 30 µg)		5	10	10	6	2	7

Note: N/A—No antibacterial activity was found with the used initial concentration.

metal ions and the direct contact effect of nanoparticles on bacterial cells.⁸⁷ Since, the pectin-Ag nanocomposite was incorporated into the PVA polymer matrix, which excludes direct contact with pathogen cells, we suppose that the mechanism of the antibacterial action of pectin-Ag/PVA films was due to the diffusion of silver ions without leaching of Ag nanoparticles from the films. Francis et al.⁸⁸ proved the similar mechanism for PVA films containing CuO and ZnO nanoparticles by inductively coupled plasma-optical emission spectrometry and energy-dispersive X-ray spectroscopy. According to⁸⁹ the slow but prolonged Ag⁺ release from film-embedded pectin-Ag nanocomposite (8%–11% of total Ag released after 24 h) resulted in a very strong microbicidal effect against planktonic *E. coli* and *S. aureus* bacterial strains.

Silver nanoparticles could be considered as a silver ions depot, the release kinetics of which depends on the

size of nanoparticles, functionalization of their surface, temperature, and composition of the medium.^{90,91} Nanoparticles release ions by slow oxidation via oxygen present in the moist environment of the growth medium. In addition, acidification of the environment by uptake of CO₂ from the ambient air or by metabolites released by bacteria can enhance the dissolution of Ag metal.⁹⁰ Silver ions have a strong bactericidal effect mainly due to interactions with thiol and amino groups of proteins, with nucleic acids, and with cell membranes.^{91,92} Moreover, the smaller the size of silver particles, the greater the local concentration of silver ions was registered.⁹³ Authors⁹⁰ supposed, that high release rate of Ag⁺ by small nanosilver particles (≤10 nm) could be related to their high specific surface area and enhanced curvature that facilitates mass transfer from their surface (Kelvin effect) and/or the presence of an oxide layer on the nanosilver surface.

TABLE 6 Antibacterial activity of pectin-Ag/PVA/KAN films

Pectin-Ag	Mw PVA	<i>B. subtilis</i> B-25	<i>B. subtilis</i> B-210	<i>B. pumilus</i> B-211	<i>B. pumilus</i> B-373	<i>P. aeruginosa</i> B-153	<i>E. coli</i> B-378
Citrus-Ag	30,000	6	15	8	15	10	10
	66,000	7	15	9	15	7	9
	145,000	7	15	9	15	8	10
Classic-Ag	30,000	12	15	10	7	7	10
	66,000	10	16	9	6	10	9
	145,000	8	15	9	5	8	10
Amid-Ag	30,000	7	full inhibition	>10	>10	7	10
	66,000	9		>10	>10	10	9
	145,000	7		>10	>10	9	10

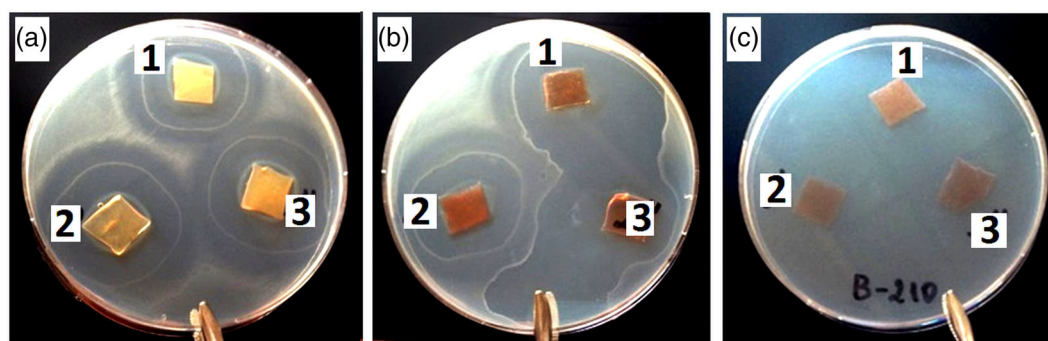


FIGURE 11 *B. subtilis* B-210 inhibition zones of KAN-containing films based on citrus-Ag (a), classic-Ag (b), amid-Ag (c) nanocomposite. PVA molecular weight was 30,000 (1), 66,000 (2) and 145,000 (3). [Color figure can be viewed at wileyonlinelibrary.com]

2.13 | Antibacterial activity of kanamycin-containing pectin-Ag/PVA films against gram-positive bacteria strains

Regardless of the type of nanocomposite and PVA molecular weight, pectin-Ag/PVA films containing kanamycin showed more pronounced antimicrobial activity against selected gram-positive bacteria of the genus *Bacillus*, except for *B. pumilus* (for Citrus-Ag and Classic-Ag), compared with initial pectin-Ag/PVA films and, in some cases, it resulted in full inhibition of bacterial growth (Table 6, Figure 11). Pectin-Ag/PVA/KAN films even retarded growth of resistant bacteria strain *B. subtilis* BIM B-25.

It should be noted that Amid-Ag/PVA/KAN films had the highest antibacterial activity against *B. subtilis* BIM-210, *B. pumilus* BIM B-211, and *B. pumilus* BIM B-373.

2.14 | Antibacterial activity of films against gram-negative KAN-sensitive and KAN-resistant bacteria strains

The films based on nanocomposites did not exhibit antibacterial properties against strains of gram-negative bacteria

Pseudomonas aeruginosa BIM B-153 and *Escherichia coli* BIM B-378 (Table 5). However, KAN-containing films produced statistically significant inhibition zones of bacterial growth (Table 6). The size of inhibition zone for *Pseudomonas aeruginosa* BIM B-153 was 7–10 mm. Antibacterial activity of the films against strain *Escherichia coli* BIM B-378 was even more evident (Table 6).

In addition, KAN-containing films induced significant zones of growth inhibition of *P. aeruginosa* B-807 (Figure 12) and B-994 strains which are resistant to KAN. The films based on Amid-Ag showed the lowest antibacterial effect: the inhibition zone was only 1.5–2.5 mm. In case of Citrus-Ag/PVA/KAN and Classic-Ag/PVA/KAN films, the inhibition zone reached 5–6 mm. This striking difference is due to the fact that kanamycin in films is available in native and bound (to pectin-Ag) forms. It was established that percentage of KAN binding to pectin-Ag nanocomposites is variable and depends on the type of nanocomposite (Figure 13).

The amount of bound KAN decreases from 67.8 ± 4.5 to $16.0\% \pm 3.3\%$ in the series Citrus-Ag–Classic-Ag–Amid-Ag. According to obtained FTIR and DLS data, the pectin-Ag/KAN complexes are mainly formed due to the electrostatic interaction between carboxyl groups of

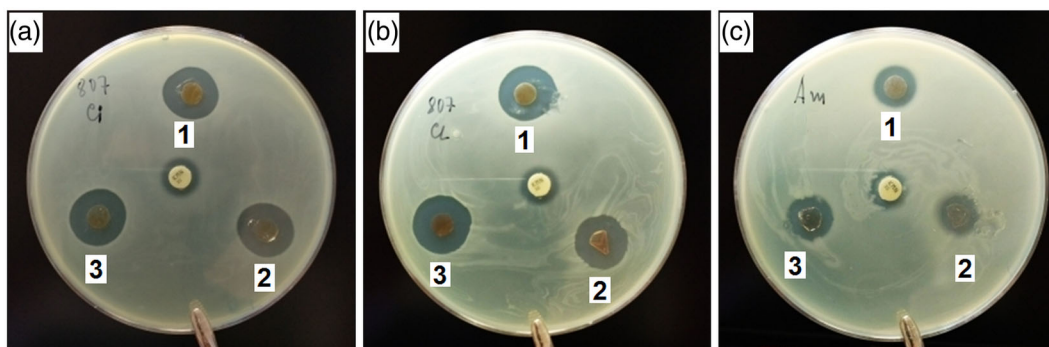


FIGURE 12 *P. aeruginosa* B-807 inhibition zones of KAN-containing films based on citrus-Ag (a), classic-Ag (b), amid-Ag (c) nanocomposite. PVA molecular weight was 30,000 (1), 66,000 (2) and 145,000 (3). Standard kanamycin disk—in the center. [Color figure can be viewed at wileyonlinelibrary.com]

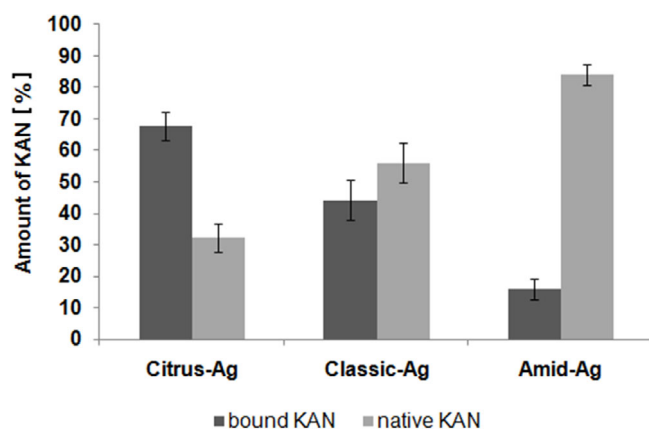


FIGURE 13 Binding of kanamycin to pectin-Ag nanocomposite

pectin-Ag and amino groups of KAN. Thus, the lowest percentage of KAN binding for Amid-Ag is attributed to the smaller number of free COOH groups. In view of the above, Amid-Ag/PVA/KAN films compared to other films contain the larger amount of native kanamycin not entrapped in the complex. Therefore, in case of KAN-sensitive strains, these films were characterized by the highest inhibitory effect owing to the maximum concentration of native kanamycin enhanced by the impact of the Amid-Ag/KAN complex. On the contrary, minimal inhibitory effect was observed in case of KAN-resistant strains (Figure 12), because kanamycin in the native form proved ineffective and the concentration of pectin-Ag/KAN complex was minimal compared with Citrus-Ag/PVA/KAN and Classic-Ag/PVA/KAN films.

The enhancement of the antibacterial activity of kanamycin-containing films corresponds to the literature data. It is known that among bactericidal and bacteriostatic antibiotics, including tetracycline and chloramphenicol, silver ions most effectively enhance the toxic effect of aminoglycosides (minimum inhibitory concentration is reduced

by 10 or more times).⁹⁴ The similar effect was also observed for metallic silver nanoparticles. Authors⁹⁵ reported an increase in the antibacterial effect for kanamycin adsorbed on silver NPs compared with individual components against clinically important pathogenic (*S. aureus*, *B. megaterium*, *P. vulgaris*, and *S. sonnei*) and non-pathogenic (*B. subtilis* and *P. fluorescens*) strains. Synergistic and additive antibacterial effects were proven for combinations of chitosan-silver nanobiocomposite with azithromycin, levofloxacin, and tetracycline against gram-negative and gram-positive bacterial strains.⁹⁶ The authors proved the adsorptions of the drugs on the silver surfaces using Raman and SERS spectroscopy, therefore, polysaccharide-silver nanobiocomposites could be considered as carriers of drugs. And this silver-drug interaction provides the decrease in the minimum inhibitory concentration of the drugs by 37%–97%.

Finally, the experimentally established fact of the action of kanamycin-containing films against antibiotic-resistant *P. aeruginosa* strains is also in agreement with the literature data. The authors^{92,97} showed that silver disrupts multiple bacterial cellular processes and destabilizes the membrane in a protein translation-dependent pathway. These changes cause the increase in production of reactive oxygen species and improve membrane permeability of gram-negative bacteria that can enhance the antimicrobial activity of antibiotics, as well as restore antibiotic susceptibility to a resistant bacteria strain.⁹⁷ Indeed, silver ions could restore antibiotic susceptibility to a tetracycline resistant *E. coli* mutant⁹⁷ and Ag nanoparticles assisted revival of streptomycin against multi-drug resistant strain *S. aureus*.⁹⁸

3 | CONCLUSION

In this study, pectin-Ag nanocomposites with size of 10–30 nm were synthesized by “green chemistry” method at

room temperature. A comparative study of the structural organization, mechanical and antimicrobial properties of PVA films with incorporated pectin-Ag nanocomposites has been carried out. The pectin-Ag/PVA films showed attractive mechanical (strength, flexibility) and optical (transparency) characteristics, which makes them promising materials for biomedical and food applications. It was demonstrated that the antimicrobial properties of pectin-Ag/PVA films correlate with the size of embedded silver nanoparticles. The obtained results showed that PVA films containing smaller Ag nanoparticles, on average, exhibited antimicrobial activity against gram-positive spore-forming bacteria of the genus *Bacillus* comparable or even higher than kanamycin activity. The films based on pectin-Ag nanocomposites can be used to entrap kanamycin, prolong its release, and can provide the antimicrobial effect against gram-positive and gram-negative bacteria. The mechanism of antibacterial activity of KAN-containing films is related with the formation of ionic complexes between antibiotic and pectin-Ag nanocomposite. Finally, we have demonstrated that the obtained pectin-Ag/PVA films containing kanamycin are effective against resistant microbial strains and, therefore, can be used as wound dressings.

4 | MATERIALS AND METHODS

4.1 | Materials

Silver nitrate (AgNO_3 , Sigma-Aldrich), kanamycin sulfate (KAN, Sigma-Aldrich), sodium hydroxide, sulfuric acid, phenol were purchased and used in further studies. Pectins with different degrees of esterification (DE) and amidation (DA) (Citrus, DE 71%, $M_v \sim 141,000$, Sigma-Aldrich; Amid, DE 32%, DA 18%, $M_v \sim 120,000$, Herbstreith and Fox; Classic, DE 35%–42%, $M_v \sim 89,000$, Herbstreith and Fox) were used for preparation of pectin-Ag nanocomposites. Polyvinyl alcohol (PVA 30000, $M_w \sim 30,000$, degree of hydrolysis [DH] $\geq 98\%$, Merck; PVA 66000, $M_w \sim 66,000$, DH $\geq 99\%$, Japan; PVA 145000, Mowiol 28–99, $M_w \sim 145,000$, DH 99%) was used for preparation of pectin-Ag/PVA films. Glycerol (purity 99%) was purchased from AppliChem (Germany). All aqueous solutions were prepared with distilled water.

4.2 | Preparation of pectin-Ag nanocomposites

Pectin-Ag nanocomposites were synthesized by «green chemistry» method^{36,37} with slight modification. The freshly prepared aqueous 2.0 mM AgNO_3 solution (10 ml) was added to

an aqueous pectin solution (100 ml) under stirring with a magnetic stirrer and left thereafter for 10 min. Then, a 3.0% sodium hydroxide solution (3.4 ml) was added to the reaction mixture under intensive stirring. After 6 h, the synthesized pectin-Ag nanocomposite was purified by dialysis against distilled water. Thus, three types of pectin-Ag nanocomposites were obtained: Citrus-Ag, Classic-Ag, and Amid-Ag.

The amount of unreacted Ag^+ after synthesis was measured by Atomic Absorption Spectroscopy. Once the reaction is over, the obtained hydrosol of silver nanoparticles coated with pectin (113.4 ml) was placed in a dialysis tubing cellulose membrane. The dialysis was carried out three times against distilled water (2 L) and water samples were collected. The concentration of Ag^+ in dialysis water was determined using High-Resolution Continuum Source Flame Atomic Absorption Spectrometer ContrAA 300 (Analytik Jena AG, Jena, Germany), equipped with a xenon short-arc lamp. Acetylene flame (C_2H_2) was used for atomization of Ag^+ .

It was determined that amount of silver ions in dialysis water was less 1%. So, the Ag content of pectin/Ag nanocomposite is app. Equal the Ag content of initial salt (AgNO_3).

4.3 | Preparation of pectin-Ag/PVA films

The pectin-Ag/PVA films were prepared by a casting evaporation technique from aqueous polymer solutions: pectin-Ag nanocomposite hydrosol and 3.0% PVA solution of different molecular weight were premixed. The glycerol was used as a plasticizer in the ratio (w/w) PVA: glycerol = 2:1. The mixture (10 ml of pectin/Ag nanocomposite and 10 g of PVA solution) was poured into 90 mm Petri dishes and dried at $50.0 \pm 2.0^\circ\text{C}$ for 18 h. The final silver concentration in the film was 0.05 mg cm^{-2} .

Antibiotic-containing films were prepared by adding a KAN aqueous solution to the mixture of pectin-Ag nanocomposite and PVA. The mixture was poured into 90 mm Petri dishes and dried at $50.0 \pm 2.0^\circ\text{C}$ for 18 h. The final KAN concentration in the films was 1.0 mg cm^{-2} .

4.4 | Binding of kanamycin to pectin-Ag nanocomposite

Pectin-Ag hydrosols were mixed with KAN solution (15.0 mg ml^{-1}) for at least 1 h. To separate native KAN from AgNP bound form, the mixture was dialyzed against distilled water for 24 h. Then, amount of native KAN in dialysis water was determined by Molisch's test described in the previous study.⁴² Test solution (1 ml) was mixed with 2.5% aqueous solution of phenol (1 ml) and

concentrated sulfuric acid (5 ml). After 10 min the absorption spectrum of the mixture was recorded using spectrofluorimeter CM2203 (Solar, Belarus). Concentration of KAN was determined from calibration curve $A_{\lambda = 480} = f(C_{KAN})$. All KAN binding experiments were repeated three times.

4.5 | Degradation of pectin-Ag/PVA films

The film degradation was studied in vitro in the phosphate buffered saline (PBS, pH 7.4) solution at 37.0°C for 28 days. The samples were incubated in tenfold volumes of PBS, after definite time intervals (1, 7, 14, 21, and 28 days) the films were evacuated from the buffer, the excess solution was removed with filter paper and films were dried and weighed. All experiments were carried out three times.

4.6 | Kanamycin release from pectin-Ag/PVA/KAN films

The KAN release from the films in physiological solution (0.9% NaCl) at 37.0°C was investigated using dialysis tubing cellulose membrane (14,000 Da, Sigma-Aldrich). The amount of released antibiotic was determined by Molisch's test as previously described in Section 2.4. Data presented were averaged for duplicate measurements.

4.7 | Antimicrobial activity of pectin-Ag/PVA and pectin-Ag/PVA/KAN films

Antimicrobial properties of the films were estimated by an agar diffusion test. The samples (10 × 10, or Ø 6 mm in case of KAN-resistant bacteria strains) were placed in Petri dishes with nutrient agar inoculated with the suspension of microorganisms (concentration 1.0×10^8 CFU ml⁻¹). The samples were tested against gram-negative bacteria *Escherichia coli* and *Pseudomonas aeruginosa*, gram-positive bacteria *Bacillus pumilus*, and *Bacillus subtilis*. After incubation period (24 h at 37.0°C) the samples were visually analyzed by measuring inhibition zones (mm), that is, the distance from the edge of the sample to the border of bacterial growth.

4.8 | Instrumentation

Average hydrodynamic diameter (d_H) of the AgNPs and their complexes with KAN was measured by dynamic

light scattering (DLS) technique using Zetasizer Nano-ZS analyzer (Malvern, UK). ξ -potential values of AgNPs were calculated from the Smoluchowski equation on the basis of electrophoretic mobility data obtained by Zetasizer Nano-ZS analyzer (Malvern, UK).

Shape and size of AgNPs were determined by transmission electron microscopy (TEM) using JEOL-LEM-1400 unit (Jeol Ltd., Tokyo, Japan). TEM samples were prepared by dropping colloidal solution onto a copper grid with collodium layer and drying in the air.

Film thickness was measured at 10 positions by coating thickness gauge TT220 (TIME Group Inc., China) and the mean thickness was calculated.

Transparency of the films was estimated by light transmission through the samples in the wavelength range 400–800 nm using UV-Vis spectrofluorimeter CM2203 (Solar, Belarus). Data presented were averaged for duplicate measurements.

Surface plasmon resonance (SPR) spectra of nanocomposites and films were recorded using spectrofluorimeter CM2203 (Solar, Belarus) from 350 to 700 nm at room temperature.

Fourier transform infrared spectra (FTIR) of the obtained pectin-Ag/PVA and pectin-Ag/PVA/KAN films were recorded using Tensor 27 FTIR spectrometer (BRUKER, Germany) by scanning along spectrum range from 4000 to 400 cm⁻¹. Structure of the samples was evaluated by attenuated total reflection (ATR) infrared spectroscopy using Tensor 27 FTIR spectrometer equipped with diamond ATR unit. Data collection was performed with a 4 cm⁻¹ spectral resolution and 32 scans.

Tensile strength (TS) and elongation at break (EB) were measured with an Instron Universal Testing Machine (Instron Tensometer 2020). Deformation rate–100 mm min⁻¹. The standard film strips 150 mm long and 25 mm wide were used. TS and EB tests were replicated at least three times for each type of films.

4.9 | Statistical analysis

Results were presented as mean ± SD. The statistical analysis of the obtained data was performed using the one-way analysis of variance (ANOVA) with a significant level of $p = 0.05$. The value of $p < 0.05$ was considered to be statistically significant.

AUTHOR CONTRIBUTIONS

Aliaksandr Kraskouski: Investigation (equal); writing – original draft (equal); writing – review and editing (equal). **Kseniya Hileuskaya:** Conceptualization (lead); writing – original draft (equal). **Alena Ladutska:** Investigation (equal). **Volha Kabanava:** Investigation (equal).

Aliaksandr Liubimau: Investigation (equal). **Galina Novik:** Supervision (equal). **Tran Thi Y. Nhi:** Investigation (equal). **Vladimir Agabekov:** Supervision (equal).

ACKNOWLEDGMENTS

This study was financially supported by Belarusian Republican Foundation for Fundamental Research (grant no. B21V-002/01) and Vietnamese Academy of Science and Technology (Code QTBY01.01/21-22).

CONFLICT OF INTEREST

The authors declare no conflicts of interest.

DATA AVAILABILITY STATEMENT

The data that support the findings of this study are available from the corresponding author upon reasonable request.

ORCID

Aliaksandr Kraskouski  <https://orcid.org/0000-0002-4626-4533>

REFERENCES

- [1] Antimicrobial Resistance Collaborators, *The Lancet*. **2022**, 399, 629.
- [2] C.-W. Chen, C.-Y. Hsu, S.-M. Lai, W.-J. Syu, T.-Y. Wang, P.-S. Lai, *Adv. Drug Delivery Rev.* **2014**, 78, 88.
- [3] P. Singh, A. Garg, S. Pandit, V. Mokkaapati, I. Mijakovic, *Nanomaterials (Basel)*. **2018**, 8, 1009.
- [4] S. Mahmoodi, A. Elmi, S. Hallaj Nezhadi, *J. Mol. Pharm. Org. Process Res.* **2018**, 6, 1000140.
- [5] X. Li, S. M. Robinson, A. Gupta, K. Saha, Z. Jiang, D. F. Moyano, V. M. Rotello, *ACS Nano* **2014**, 8, 10682.
- [6] S. M. Dizaj, F. Lotfipour, M. Barzegar-Jalali, M. H. Zarrintan, K. Adibkia, *Mater. Sci. Eng. C*. **2014**, 44, 278.
- [7] R. A. Bapat, T. V. Chaubal, C. P. Joshi, P. R. Bapat, H. Choudhury, M. Pandey, B. Gorain, P. Kesharwani, *Mater. Sci. Eng. C*. **2018**, 91, 881.
- [8] S. P. Deshmukh, S. M. Patil, S. B. Mullani, S. D. Delekar, *Mater. Sci. Eng. C*. **2019**, 97, 954.
- [9] J. Molling, J. Seezink, B. Teunissen, I. Muijers-Chen, P. Borm, *Nanotechnol. Sci. Appl.* **2014**, 7, 97.
- [10] Y. A. Krutyakov, A. A. Kudrinskiy, A. Y. Olenin, G. V. Lisichkin, *Russ. Chem. Rev.* **2008**, 77, 233.
- [11] J. Natsuki, T. Natsuki, Y. Hashimoto, *Int. J. Mater. Sci. Appl.* **2015**, 4, 325.
- [12] S. H. Lee, B. H. Jun, *Int. J. Mol. Sci.* **2019**, 20, 865.
- [13] S. Iravani, H. Korbekandi, S. V. Mirmohammadi, B. Zolfaghari, *RPS*. **2014**, 9, 385.
- [14] K. M. M. Abou El-Nour, A. Eftaiha, A. Al-Warthan, R. A. A. Ammar, *Arab. J. Chem.* **2010**, 3, 135.
- [15] A. Stepanov, *Rev. Adv. Mater. Sci.* **2010**, 26, 1.
- [16] O. Kylián, A. Kuzminova, R. Štefaníková, J. Hanuš, P. Solař, P. Kůš, M. Cieslar, A. Choukourov, H. Biederman, *Mater. Lett.* **2019**, 253, 238.
- [17] A. A. Menazea, *Radiat. Phys. Chem.* **2020**, 168, 108616.
- [18] K. Parveen, V. Banse, L. Ledwani, *AIP Conf. Proc.* **2016**, 1724, 020048.
- [19] K. Ranaszek-Soliwoda, E. Tomaszewska, K. Małek, G. Celichowski, P. Orłowski, M. Krzyzowska, J. Grobelny, *Colloids Surf., B* **2019**, 177, 19.
- [20] K. S. Siddiqi, A. Husen, R. A. K. Rao, *J. Nanobiotechnology*. **2018**, 16, 14.
- [21] P. Orłowski, M. Zmigrodzka, E. Tomaszewska, K. Ranaszek-Soliwoda, M. Czupryn, M. Antos-Bielska, J. Szemraj, G. Celichowski, J. Grobelny, M. Krzyzowska, *Int. J. Nanomed.* **2018**, 13, 991.
- [22] H. B. Ahmed, M. M. Mikhail, S. El-Sherbiny, K. S. Nagy, H. E. Emam, *J. Colloid Interface Sci.* **2020**, 561, 147.
- [23] H. E. Emam, M. M. Mikhail, S. El-Sherbiny, K. S. Nagy, H. B. Ahmed, *Environ. Sci. Pollut. Res.* **2020**, 27, 6459.
- [24] H. B. Ahmed, H. E. Emam, *Polym. Test.* **2020**, 89, 106720.
- [25] H. E. Emam, M. A. Attia, F. M. S. E. El-Dars, H. B. Ahmed, *J. Polym. Environ.* **2019**, 28, 553.
- [26] H. B. Ahmed, M. A. Attia, F. M. S. E. El-Dars, H. E. Emam, *Int. J. Biol. Macromol.* **2019**, 128, 214.
- [27] V. Demchenko, S. Riabov, S. Sinelnikov, O. Radchenko, S. Kobylinskiy, N. Rybalchenko, *Carbohydr. Polym.* **2020**, 242, 116431.
- [28] H. E. Emam, H. B. Ahmed, R. M. Abdelhameed, *Carbohydr. Polym.* **2021**, 266, 118163.
- [29] N. M. Sahasrabudhe, M. Beukema, L. Tian, B. Troost, J. Scholte, E. Bruininx, G. Bruggeman, M. van den Berg, A. Scheurink, H. A. Schols, M. M. Faas, P. de Vos, *Front. Immunol.* **2018**, 9, 383.
- [30] M. L. Bruschi, S. B. de Souza Ferreira, J. Bassi da Silva, Ch. 4. in *Nanotechnology for Oral Drug Delivery: From Concept to Applications* (Eds: J. P. Martins, H. A. Santos), Academic Press, London, UK **2020**.
- [31] R. V. Kumar, D. Srivastava, V. Singh, U. Kumar, V. K. Vishvakarma, P. Singh, D. Kumar, R. Kumar, *Sci. Rep.* **2020**, 10, 21789.
- [32] F. Salehi, H. Behboudi, G. Kavooosi, S. K. Ardestani, *Sci. Rep.* **2018**, 8, 13902.
- [33] R. Ciriminna, A. Fidalgo, F. Meneguzzo, A. Presentato, A. Scurria, D. Nuzzo, R. V. Alduina, L. M. Ilharco, M. Pagliaro, *ChemMedChem* **2020**, 15, 2228.
- [34] A. Noreen, Z.-H. Nazli, J. Akram, I. Rasul, A. Mansha, N. Yaqoob, R. Iqbal, S. Tabasum, M. Zuber, K. M. Zia, *Int. J. Biol. Macromol.* **2017**, 101, 254.
- [35] H. B. Ahmed, M. K. Zahran, H. E. Emam, *Int. J. Biol. Macromol.* **2016**, 91, 208.
- [36] M. K. A. Al-Muhanna, K. S. Hileuskaya, V. I. Kulikouskaya, A. N. Kraskouski, V. E. Agabekov, *Colloid J.* **2015**, 77, 677.
- [37] K. Hileuskaya, A. Ladutska, V. Kulikouskaya, A. Kraskouski, G. Novik, I. Kozerozhets, A. Kozlovskiy, V. Agabekov, *Colloids Surf. A: Physicochem. Eng. Asp.* **2020**, 585, 124141.
- [38] H. E. Emam, N. M. Saad, A. E. M. Abdallah, H. B. Ahmed, *Int. J. Biol. Macromol.* **2020**, 156, 829.
- [39] M. K. Zahran, H. B. Ahmed, M. H. El-Rafie, *Carbohydr. Polym.* **2014**, 111, 971.
- [40] Z. Hussain, H. E. Thu, M. Sohail, S. Khan, *J. Drug Deliv. Sci. Technol.* **2019**, 54, 101169. <https://doi.org/10.1016/j.jddst.2019.101169>
- [41] H. Deng, D. McShan, Y. Zhang, S. S. Sinha, Z. Arslan, P. C. Ray, H. Yu, *Environ. Sci. Technol.* **2016**, 50, 8840.

- [42] K. S. Hileuskaya, A. N. Kraskouski, A. I. Ladutska, G. I. Novik, V. E. Agabekov, *Dokl. Natl. Acad. Sci. Belarus*. **2018**, 62, 432.
- [43] J. K. Patra, K. -H. Baek, *Front. Microbiol.* **2017**, 8, 167.
- [44] S. Jamaran, B. R. Zarif, *Open J. Ecol* **2016**, 6, 452.
- [45] R. Nishanthi, S. Malathi, S. John Paul, P. Palani, *Mater. Sci. Eng. C* **2019**, 96, 693.
- [46] E. A. Kamoun, E. -R. S. Kenawy, X. Chen, *J. Adv. Res.* **2017**, 8, 217.
- [47] A. Demir, E. Cevher, *Biomater. Appl. Nanomedicine*. IntechOpen **2011**, 19, 383. <https://doi.org/10.5772/25177>
- [48] C. Adlhart, J. Verran, N. F. Azevedo, H. Olmez, M. M. Keinänen-Toivola, I. Gouveia, L. F. Melo, F. Crijns, *J. Hosp. Infect.* **2018**, 99, 239.
- [49] T. Kruk, K. Szczepanowicz, D. Kręgiel, L. Szyk-Warszyńska, P. Warszyński, *Colloids Surf., B* **2016**, 137, 158.
- [50] M. Borzenkov, M. Moros, C. Tortiglione, S. Bertoldi, N. Contessi, S. Faré, A. Taglietti, A. D'Agostino, P. Pallavicini, M. Collini, G. Chirico, *Beilstein J. Nanotechnol.* **2018**, 9, 2040.
- [51] V. N. Popok, C. M. Jeppesen, P. Fojan, A. Kuzminova, J. Hanuš, O. Kylián, *Beilstein J. Nanotechnol.* **2018**, 9, 861.
- [52] J. V. Meshram, V. B. Koli, M. R. Phadatare, S. H. Pawar, *Mater. Sci. Eng. C* **2017**, 73, 257.
- [53] M. Dhanasekar, V. Jenefer, R. B. Nambiar, S. G. Babu, S. P. Selvam, B. Neppolian, S. V. Bhat, *Mater. Res. Bull.* **2018**, 97, 238.
- [54] J. Chen, D. Wei, W. Gong, A. Zheng, Y. Guan, A. C. S. Appl, *Mater. Interfaces*. **2018**, 10, 43.
- [55] I. Liakos, L. Rizzello, I. S. Bayer, P. P. Pompa, R. Cingolani, A. Athanassiou, *Carbohydr. Polym.* **2013**, 92, 176.
- [56] I. P. Merlusca, D. S. Matiut, G. Lisa, M. Sillion, L. Gradinaru, S. Oprea, I. M. Popa, *Polym. Bull.* **2017**, 75, 3971.
- [57] S. Pavlukhina, I. Zhuk, A. Mentbayeva, E. Rautenberg, W. Chang, X. Yu, B. Belt-Gritter, H. J. Busscher, H. C. Mei, S. A. Sukhishvili, *NPG Asia Mater.* **2014**, 6, e121.
- [58] V. G. L. Souza, C. Rodrigues, L. Ferreira, J. R. A. Pires, M. P. Duarte, I. Coelho, A. L. Fernando, *Ind. Crops Prod.* **2019**, 140, 111563.
- [59] N. Vahedikia, F. Garavand, B. Tajeddin, I. Cacciotti, S. M. Jafari, T. Omid, Z. Zahedi, *Colloids Surf., B* **2019**, 177, 25.
- [60] I. Liakos, L. Rizzello, D. J. Scurr, P. P. Pompa, I. S. Bayer, A. Athanassiou, *Int. J. Pharm.* **2014**, 463, 137.
- [61] Z. Zhang, Y. Wu, Z. Wang, X. Zhang, Y. Zhao, L. Sun, *Mater. Sci. Eng. C* **2017**, 78, 706.
- [62] F. E. F. Silva, K. A. Batista, M. C. B. Di-Medeiros, C. N. S. Silva, B. R. Moreira, K. F. Fernandes, *Mater. Sci. Eng. C* **2016**, 58, 927.
- [63] D. Hu, L. Wang, *React. Funct. Polym.* **2016**, 101, 90.
- [64] A. Kraskouski, K. Hileuskaya, V. Kulikouskaya, S. Pinchuk, I. Vasilevich, V. Kabanava, T. Kuznetsova, V. Lapitskaya, V. Agabekov, I. Volotovskii, *J. Biomed. Mater. Res. A* **2021**, 109, 1379.
- [65] R. Niranjana, M. Kaushik, J. Prakash, K. S. Venkataprasanna, A. Christy, B. Pannarselvam, G. D. Venkatasubbu, *Colloids Surf., B* **2019**, 182, 110339.
- [66] N. Jain, V. Singh, S. Chauhan, *J. Mech. Behav. Mater.* **2018**, 26, 213.
- [67] P. Pallavicini, C. R. Arciola, F. Bertoglio, S. Curtosi, G. Dacarro, A. D'Agostino, F. Ferrari, D. Merli, C. Milanese, S. Rossi, A. Taglietti, M. Tenci, L. Visai, *J. Colloid Interface Sci.* **2017**, 498, 271.
- [68] V. L. Demchenko, S. M. Kobylinskyi, S. V. Riabov, V. I. Shtompel, M. V. Iurzhenko, N. P. Rybalchenko, *Appl. Nanosci.* **2020**, 10, 5409.
- [69] H. Kaczmarek, A. Da, browska, I. Vuković-Kwiatkowska, *J. Appl. Polym. Sci.* **2011**, 122, 1936.
- [70] N. Ardjoum, S. Shankar, N. Chibani, S. Salmieri, M. Lacroix, *Food Hydrocolloids* **2021**, 121, 107000.
- [71] L. C. Bichara, P. E. Alvarez, M. V. Fiori Bimbi, H. Vaca, C. Gervasi, S. A. Brandán, *Infrared Phys. Technol.* **2016**, 76, 315.
- [72] V. I. Kulikouskaya, M. E. Lazouskaya, V. E. Agabekov, *Theor. Exp. Chem.* **2019**, 54, 375.
- [73] J. -S. Lee, E. -S. Lee, J. Han, *Sci. Rep.* **2020**, 10, 13622.
- [74] T. Phupoksakul, M. Leuangsupakorn, A. Somwangthanaroj, K. Tananuwan, T. Janjarasskul, *J. Appl. Polym. Sci.* **2016**, 133, 43547.
- [75] C. Gao, E. Pollet, L. Avérous, *Food Hydrocolloids* **2017**, 63, 414.
- [76] D. K. Buslov, N. I. Sushko, O. N. Tretinnikov, *Polym. Sci. Ser. A* **2011**, 53, 1121.
- [77] D. Harpaz, T. Axelrod, A. Yitian, E. Eltzov, R. S. Marks, A. I. Y. Tok, *Materials*. **2019**, 12, 343.
- [78] F. G. Torres, O. P. Troncoso, C. Torres, D. A. Diaz, E. Amaya, *Int. J. Biol. Macromol.* **2011**, 48, 603.
- [79] D. Merino, V. A. Alvarez, *Adv. Mater. Lett.* **2019**, 10, 907.
- [80] H. Ostadi, S. G. Hakimabadi, F. Nabavi, M. Vossoughi, I. Alemzadeh, *Polym. Renew. Resour.* **2020**, 11, 15.
- [81] N. Limpan, T. Prodpran, S. Benjakul, S. Prasarnpran, *Food Hydrocolloids* **2012**, 29, 226.
- [82] I. Nugrahani, R. Fauzia, *Int. J. Appl. Pharm.* **2019**, 11, 426.
- [83] A. -L. Kubo, I. Capjak, I. V. Vrček, O. M. Bondarenko, I. Kurvet, H. Vija, A. Ivask, K. Kasemets, A. Kahru, *Colloids Surf., B* **2018**, 170, 401.
- [84] Q. Xu, L. Jin, Y. Wang, H. Chen, M. Qin, *Cellulose* **2019**, 26, 1309.
- [85] M. Iqbal, H. Zafar, A. Mahmood, M. B. K. Niazi, M. W. Aslam, *Polymer* **2020**, 12, 2112.
- [86] T. Galya, V. Sedlářik, I. Kuřitka, R. Novotný, J. Sedlářiková, P. Saha, *J. Appl. Polym. Sci.* **2008**, 110, 3178.
- [87] S. Nakamura, M. Sato, Y. Sato, N. Ando, T. Takayama, M. Fujita, M. Ishihara, *Int. J. Mol. Sci.* **2019**, 20, 3620.
- [88] D. V. Francis, S. Thaliyakattil, L. Cherian, N. Sood, T. Gokhale, *Polymer* **2022**, 14, 1379.
- [89] P. Grisoli, L. De Vita, C. Milanese, A. Taglietti, Y. Diaz Fernandez, M. Bouzin, L. D'Alfonso, L. Sironi, S. Rossi, B. Vigani, P. Sperandio, A. Polissi, P. Pallavicini, *Nanomater.* **2021**, 11, 1387.
- [90] K. Fujiwara, G. A. Sotiriou, S. E. Pratsinis, *Langmuir* **2015**, 31, 5284.
- [91] S. Chernousova, M. Eppele, *Angew. Chem., Int. Ed.* **2012**, 52, 1636.
- [92] F. Barras, L. Aussel, B. Ezraty, *Antibiotics* **2018**, 7, 79.

- [93] G. A. Sotiriou, S. E. Pratsinis, *Environ. Sci. Technol.* **2010**, *44*, 5649.
- [94] M. Herisse, Y. Duverger, I. Martin-Verstraete, F. Barras, B. Ezraty, *Mol. Microbiol.* **2017**, *105*, 115.
- [95] C. Khurana, A. K. Vala, N. Andhariya, O. P. Pandey, B. Chudasama, *IET Nanobiotechnol.* **2016**, *10*, 69.
- [96] M. Brasil, A. Filgueiras, M. Campos, M. Neves, M. Eugênio, L. Sena, C. Sant'Anna, V. da Silva, C. Diniz, A. Sant'Ana, *J. Braz. Chem. Soc.* **2018**, *29*, 2026.
- [97] J. R. Morones-Ramirez, J. A. Winkler, C. S. Spina, J. J. Collins, *Sci. Transl. Med.* **2013**, *5*, 190ra81.
- [98] N. Ghaffar, S. Javad, M. A. Farrukh, A. A. Shah, M. K. Gatasheh, B. M. A. AL-Munqedhi, O. Chaudhry, *PLoS One* **2022**, *17*, e0264588.

SUPPORTING INFORMATION

Additional supporting information can be found online in the Supporting Information section at the end of this article.

How to cite this article: A. Kraskouski, K. Hileuskaya, A. Ladutska, V. Kabanava, A. Liubimau, G. Novik, T. T. Y. Nhi, V. Agabekov, *J. Appl. Polym. Sci.* **2022**, e53023. <https://doi.org/10.1002/app.53023>